ADVANCED MATERIALS TECHNOLOGIES
www.advmattechnol.de

A Compact Full 2π Flexoelectro-Optic Liquid Crystal Phase Modulator

Xiuze Wang, Julian A. J. Fells, Yuping Shi, Taimoor Ali, Chris Welch, Georg H. Mehl, Timothy D. Wilkinson, Martin J. Booth, Stephen M. Morris, and Steve J. Elston*

Wavefront shaping, which is often achieved using liquid crystal (LC) spatial light modulators, is particularly important for a wide range of applications including laser microfabrication and micromanipulation, microscopy, and quantum optics. In this work, results are presented for the first integrated LC phase modulator that combines a flexoelectro-optic LC layer (that behaves as a switchable $\lambda/2$ waveplate) with a polymerized reactive mesogen layer (which acts as a $\lambda/4$ waveplate) and a mirrored substrate that creates a double-pass geometry. For a flexoelectro-optic LC layer that exhibits switching angles of ±45° at a voltage of ±85 V a full 2π phase modulation is observed when driven by a 1 kHz waveform. Experimental results are also compared with modeling using Jones calculus of the amplitude and phase variation when the LC and the polymer layer deviate from their desired waveplate conditions. The development and demonstration of an integrated device is particularly significant for applications where size and cost are critical factors such as in LiDAR for the Space and Automotive industries, respectively.

Applications such as holography, beam steering and shaping, aberration correction, and super-resolution optical microscopy rely heavily upon technologies such as optical phase modulators.[1–5] Several technologies exist that can be used to modulate the phase of light, such as optical microelectromechanical systems (MEMS) and liquid crystal (LC)-based spatial light modulators (SLMs). While optical MEMS-based phase modulators generally exhibit very fast response times, they are often characterized by a low number of pixels, making it more challenging to accurately compensate for higher order aberrations.[6] LC materials, on the other hand, can exhibit a variety of electro-optic effects. By combining the merits of high-performance complementary metal oxide semiconductor (CMOS) technology with the various electro-optical properties of LC materials, LC-based SLM technologies are able to support a large number of pixels to provide high resolution across a wave-front in a compact technology. This high-resolution is a key advantage of LC-based SLMs in comparison with other technologies. However, the technology often suffers from either slow response times (nematic LC) or binary phase modulation (chiral smectic C).[7–10]

Approaches based upon 2D materials have been considered as an alternative candidate for phase modulation technology.[11–14] As examples, an 8π phase range all-optical phase modulator has been reported which relies on using a strong photothermal effect in phosphorene[11] whereas an antimonene-based optical modulator has been developed that can provide fast phase (up to 16π) and intensity modulation at the same time.[14] However, these technologies still have their limitations such as relatively slow response times (e.g., milliseconds) or relatively high pump powers, which may not be desirable for some practical applications. Developing new types of phase modulators that possess fast response, analog phase modulation, and low driving voltage is particularly important for applications such as beam-steering in optical communications[3] and real-time holography.[15]

Flexoelectro-optic chiral nematic LCs have been shown to be a promising candidate for phase modulation owing to the fast-switching times and the analog control of the tilt angle of the optic axis.[16] The flexoelectro-optic effect can be observed when an electric field is applied perpendicular to the helical axis, resulting in a deflection of the optic axis from the unperturbed helical axis in a plane that is orthogonal to the applied field direction.[17–22] For conventional devices with transverse electrodes, a uniform lying helix (ULH) geometry is required to ensure that the field direction is orthogonal to the helix axis. The response time of the flexoelectro-optic effect can be of the order of 100s of microseconds when the pitch of the chiral nematic LC is short (<500 nm).

X. Wang, Dr. J. A. J. Fells, Y. Shi, T. Ali, Prof. M. J. Booth, Prof. S. M. Morris, Prof. S. J. Elston
Department of Engineering Science
University of Oxford
Parks Road, Oxford OX1 3PJ, UK
E-mail: stephen.morris@eng.ox.ac.uk

Dr. C. Welch, Prof. G. H. Mehl
Department of Chemistry
University of Hull
Hull HU6 7RX, UK

Prof. T. D. Wilkinson
Department of Engineering
University of Cambridge
9 JJ Thomson Avenue, Cambridge CB3 0FA, UK

The ORCID identification number(s) for the author(s) of this article can be found under https://doi.org/10.1002/admt.202000589.

DOI: 10.1002/admt.202000589

Recent work has shown that the flexoelectro-optic effect can be used to achieve full 2π phase modulation when chiral nematic LCs with large tilt angles (>45°) of the optic axis are combined with a $\lambda/4$ waveplate and a reflector that both preserves the handedness of circularly polarized light and creates a double-pass geometry.[23,24] The optical field component of the light at the output of the device (E_{out}) after passing through all of the optical components can be expressed in terms of the input optical field component (E_{in}) as $E_{out} = E_{in}\, e^{+4i\varphi}$, where the total phase change is four times the switching angle, φ. Therefore, a 45° tilt angle, which equates to $\varphi = \pm 45°$ (as the optic axis tilts in opposite directions for opposite polarities of the applied electric field), leads to a 2π phase modulation.

Achieving full 2π phase modulation has been made possible by the development of LC compounds such as 4′,4′-(heptane-1,7-diyl)bis(([1′,1″-biphenyl]-4″-carbo-nitrile)) (CB7CB), which exhibits switching angles in excess of ±45° when it is doped with a small concentration of high twisting power chiral dopant.[25–29] A drawback with the configurations described in refs. [23] and [24], however, is that numerous optical components were required, which makes the current arrangement impractical for many device applications as the overall thickness is rather large. For example, in ref. [23] an LC cell with a nominal gap of 5 µm was used as the tunable $\lambda/2$ waveplate and standard bench-top optical components in the form of $\lambda/4$ waveplates and mirrors were needed to build the phase modulation system. Furthermore, the numerous free-space components result in multiple interfaces and therefore unwanted reflection losses. Before this technology can be deployed into real systems, the optical components need to be integrated into a compact package so that the overall device thickness is comparable with existing SLM devices.

In this paper, a prototype-integrated phase modulator exhibiting the desired phase modulation of 2π with a frame rate of 1kHz is demonstrated by combining a flexoelectro-optic LC layer, a birefringent polymer film (which acts as the $\lambda/4$ waveplate), and a mirror all in one compact package. The reduction of the individual components into a single device represents an important step forward in terms of development toward the realization of a flexoelectro-optic optical phase modulator.

The basic structure of the integrated device is illustrated in **Figure 1**. Briefly, the device consists of (omitting the alignment layers) a 100-nm thick silver layer that is coated onto a glass substrate, a reactive mesogen polymer film (PF) that acts as a $\lambda/4$ waveplate, a tunable flexoelectro-optic LC layer that behaves as a $\lambda/2$ waveplate, and a top glass substrate that is coated with indium tin oxide (ITO). The total thickness of the device was not precisely measured, but the thickness of the region where the device shows the appropriate phase modulation has been estimated from the results presented in this paper (vide infra). The silver layer on the bottom substrate has two functions in the device: 1) it acts as a reflector for the incoming light so as to increase the modulation depth by creating a double-pass through the LC layer, and 2) it acts as the bottom electrode, which together with the top ITO electrode, facilitates the application of an electric field across the chiral nematic LC layer so as to initiate flexoelectro-optic switching.

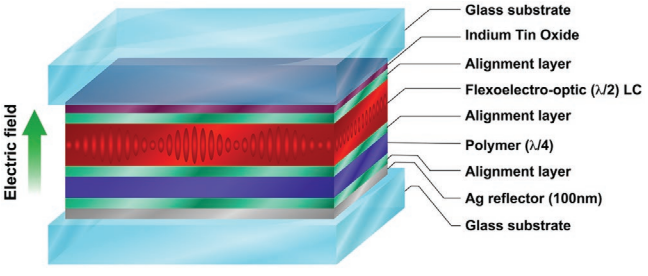

Figure 1. Device architecture of the "integrated" flexoelectro-optic LC modulator.

An experimental challenge that is encountered when fabricating the proof-of-concept device is the necessity for the polymer and LC layers to form $\lambda/4$ and $\lambda/2$ waveplates, respectively, at the desired wavelength. This requires precise control of the thickness of the layers, which is non-trivial. To relax the constraints on the thickness, the polymer and LC layers were fabricated so that each layer formed a wedge shape (as illustrated in **Figure 2**). The subsequent orientations of the wedged polymer and LC layers were orthogonal to each other, allowing a region to be found where the polymer and LC layers function as a $\lambda/4$ waveplate and a $\lambda/2$ waveplate, respectively.

The purpose of the wedge-shaped design of the PF layer and the LC layer was to enable the correct thicknesses to be found. However, this also meant that there were many different thickness combinations across the device. Deviation from the desired waveplate conditions results in both phase error and variation in the amplitude loss and to demonstrate this experimentally light was passed through a region of the device in which neither the thickness of the PF layer nor the LC layer correspond to their correct values for achieving a $\lambda/4$ and $\lambda/2$ waveplate, respectively. Toward this end, the integrated device was placed on a Michelson interferometer as shown in **Figure 3** and the measured phase and normalized amplitude loss variation from this region of the device where the waveplate conditions were not satisfied, as determined from the interference fringe images using MATLAB, are presented in **Figure 4**.

The flexoelectro-optic LC layer was modeled as a waveplate with an optic axis in a plane that is normal to the incident beam. The optical field at the output, E_{out}, of the integrated system including the linear polarizer and $\lambda/4$ waveplate (the components in the dashed blue line in Figure 3) is given by

$$E_{out} = \mathbf{P}\mathbf{Q}_1\left(-\frac{\pi}{4}\right)\mathbf{D}(-\varphi)\,\mathbf{Q}_2\left(-\frac{\pi}{4}\right)\mathbf{M}\mathbf{Q}_2\left(\frac{\pi}{4}\right)\mathbf{D}(\varphi)\,\mathbf{Q}_1\left(\frac{\pi}{4}\right)\mathbf{P}E_{in} \quad (1)$$

where E_{in} is the Jones vector for a vertically polarized light at the input, $\mathbf{P}$ is a vertically aligned linear polarizer, $\mathbf{Q}_1\left(\frac{\pi}{4}\right)$ is the Jones matrix for a $\lambda/4$ waveplate at $\pi/4$ to the vertical, $\mathbf{D}(\varphi)$ is the Jones matrix of the flexoelectro-optic LC layer with a retardance, δ, and optic axis that is oriented at an angle, φ, to the vertical axis and $\mathbf{Q}_2\left(\frac{\pi}{4}\right)$ is the Jones matrix for the PF layer, which has a retardance of ξ to allow deviation from the optimum $\lambda/4$ waveplate condition, and $\mathbf{M}$ is the Jones matrix for a mirror. Note that in the terms after the mirror (i.e., terms to the left of $\mathbf{M}$ in Equation (1)) the orientation angles of the waveplates are reversed because the system has a mirror symmetry configuration and the light is now propagating in the opposite direction.

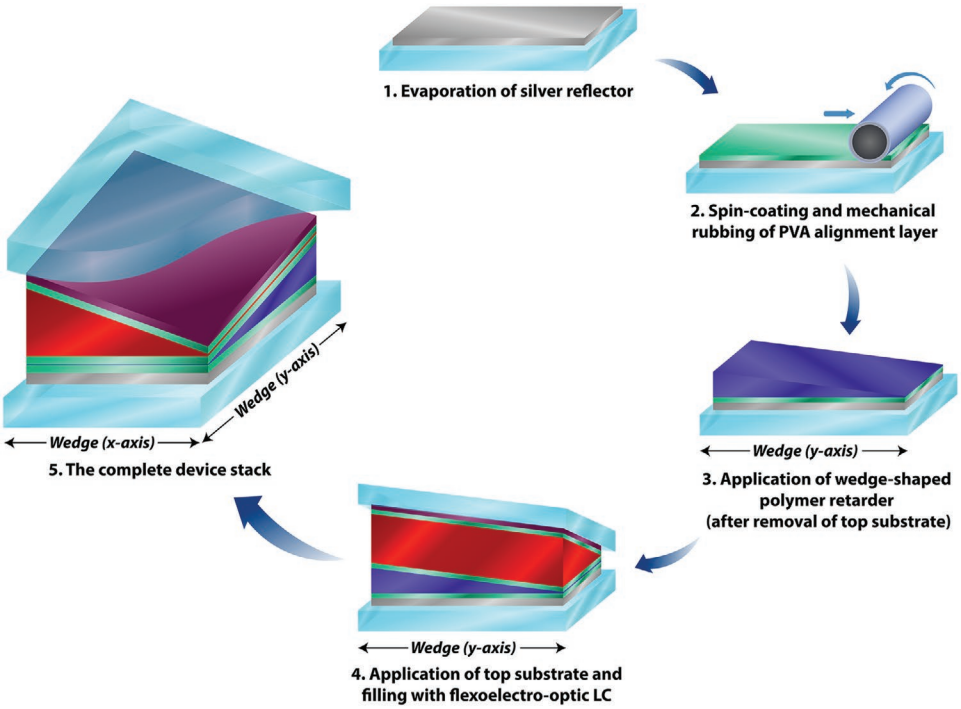

Figure 2. Schematic illustrating the key steps in the procedure for fabricating the integrated device and the formation of wedge-shaped geometries for the polymer retarder (blue layer) and flexoelectro-optic LC (red layer) layers to achieve $\lambda/4$ and $\lambda/2$ waveplate behavior, respectively. The color scheme used for the different layers is the same as that used in Figure 1.

In this example of a non-optimal region of the device, there is almost a 50% variation in the amplitude across the full range of switching angles (±45°). The red dash lines in Figure 4 shows simulated results from Equation (1), with the retardance of the PF layer set to $\xi = 0.38$ waves and the retardance of the LC layer set to $\delta = 0.8$ waves. With these values of ξ and δ, both the simulated phase and loss variation show close correlation with the experimental data. Although there is a significant deviation from the ideal values of $\xi = 0.25$ waves and $\delta = 0.5$ waves, the

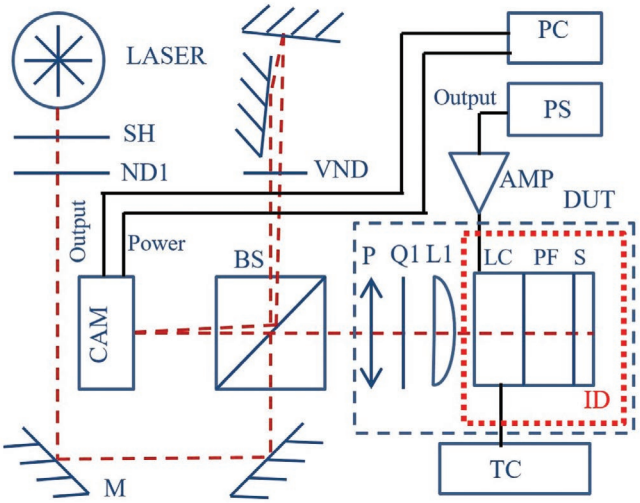

Figure 3. Michelson interferometer arrangement to measure the phase and intensity response of the integrated LC optical phase modulator: (SH) shutter; (NDX) neutral density filter of optical density X; (VND) variable neutral density filter; (PC) personal computer; (PS) power supply; (AMP) voltage amplifier; (TC) temperature controller; (CAM) CCD camera; (DUT) device under test; (P) linear polarizer; (Q1) $\lambda/4$ waveplate; (L1) lens; (LC) liquid crystal layer; (PF) reactive mesogen polymer film; (S) silvered substrate; (M) mirror; (BS) non-polarizing beam splitter. The components highlighted by the red-dashed line represent the integrated device (ID).

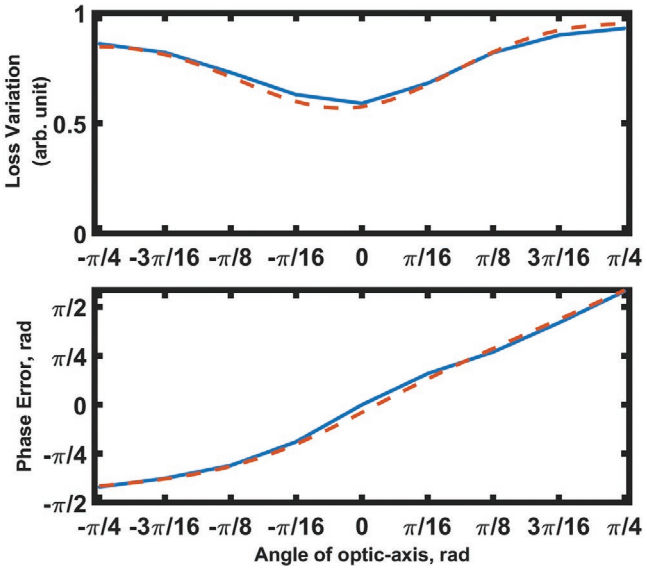

Figure 4. Experimental (blue lines) and modeling (red dashed lines) results for the amplitude loss variation and the phase error as a function of the absolute angle of the optic-axis of the flexoelectro-optic device relative to the vertical axis. These results are an example case of when the PF was not a precise $\lambda/4$ waveplate and the switchable LC layer does not fulfil the condition of a $\lambda/2$ waveplate.

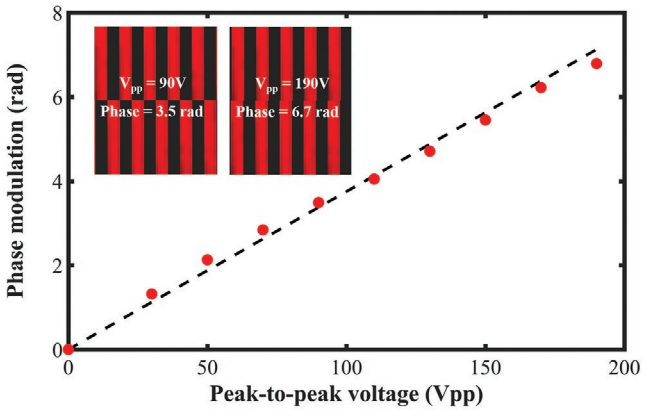

Figure 5. Experimentally determined phase for the integrated LC optical phase modulator presented in this work (measured using the Michelson interferometer presented in Figure 3). The main plot shows the optical phase shift as a function of the applied peak-to-peak voltage (Vpp). The red solid data points represent experimental measurements where the RM polymer and LC layers function as $\lambda/4$ and $\lambda/2$ waveplates, respectively, and the dashed line is a line of best fit. The inset contains an upper fringe pattern and a lower fringe pattern. Each fringe pattern corresponds to a specific voltage level and the phase difference can be obtained by comparing the position of the upper and lower fringe patterns.

device still functions as a phase modulator, but at the expense of unwanted amplitude modulation and a reduction in linearity of the phase response.

Figure 5, on the other hand, shows experimental results for light passing through an optimal area of the integrated device, where the thickness of the LC layer is close to that required for a $\lambda/2$ waveplate (nominally 5 µm) and the thickness of the PF is close to that required for a $\lambda/4$ waveplate (7 µm). Example images of the interference fringes captured on the CCD can be seen in the inset of the figure. In this exemplar case, the phase range was found to be almost 2π when the applied peak-to-peak voltage reached 170 V_{pp} (±85 V). The response time was not directly measured for this integrated device (it was faster than the frame-rate of the CCD camera). However, from the measurement of the switching times for the same mixture in a commercially-available glass test cell (Instec, 5 µm-thickness), the response time was estimated to be around 500 µs. Here the voltage required to achieve 2π is found to be substantially larger than that observed in our previous studies: it should be noted that even though the voltage is relatively large, for this switching range the ULH helix does not unwind, and therefore the changes in the birefringence are small).[23,24] The primary reason for this higher driving voltage requirement is that the thickness of the device is considerably greater than that employed in previous studies as the electric field was applied not just across the LC layer but also the $\lambda/4$ polymer retarder and the numerous alignment layers. To confirm that this was the case, the LC mixture was also filled into a commercially available glass cell (5 µm-thickness, Instec). In this case, a driving voltage of ±34 V was required to achieve ±45° switching.

The results presented in Figure 5 also show that the dependence of the phase modulation on the applied voltage follows an almost linear behavior. However, a small deviation from linearity is observed and is believed to be the combined result of a flexoelectro-optic tilt angle that is not linear with voltage at high amplitudes and small drifts in environmental temperature, which lead to measurement error. Nevertheless, the results show that by combining a reactive mesogen polymer film with a chiral nematic layer operated in a flexoelectro-optic mode it is possible to achieve full 2π modulation of the optical phase when subjected to 1 kHz switching frequencies.

There are important key characteristics of the phase modulator which we can comment on. One is the optical efficiency of the device, which was found to be around 20% to 40%, depending upon the ULH alignment quality. The relatively low efficiency is due to scattering from non-uniformities in the lying helix alignment of the LC phase modulation layer, but it is anticipated that the maximum efficiency could be significantly improved through the use of high-quality ULH alignments such as those formed using solvent-assisted processes.[30] Additionally, we can consider the Figure-of-Merit (FoM) for the modulator, as introduced by Khoo and Wu.[31] For nematic-based devices this parameter can be defined as

$$\mathrm{FoM} = \frac{K_{11}(\Delta n)^2}{\gamma_1} \tag{2}$$

where K_{11} is the LC splay elastic constant, Δn is the optical anisotropy, and γ_1 is the rotational viscosity. Unfortunately, this definition does not relate directly to the electro-optic effect that we employ in this study. However, if we note that the switching time of a nematic layer of thickness d can be characterized as

$$\tau = \frac{\gamma_1 d^2}{K_{11}\pi^2} \tag{3}$$

then we can re-write the FoM as

$$\mathrm{FoM} = \frac{1}{\tau}\cdot\frac{(\Delta n\cdot d)^2}{\pi^2} \tag{4}$$

For our device $\Delta n \cdot d$ is close to a half-wave at $\lambda = 632.8$ nm. The switching time varies with voltage, but is typically around 0.5 ms. Putting these values into Equation (4) leads to an FoM of 20 µm^2 s^{-1}. By way of comparison, for a standard nematic material, such as the eutectic mixture, E7, the FoM is found to be approximately 4 µm^2 s^{-1}. However, care must be taken when making such a comparison because the electro-optic mechanisms used are fundamentally different in the two cases. For example, in the nematic case the "switch-on" time is controlled by $\gamma_1/(\Delta\varepsilon E^2)$, where $\Delta\varepsilon$ is the dielectric anisotropy and E is the applied electric field, whereas the "switch-off" time is controlled by $\gamma_1 d^2/K_{11}$,[32] so the switch-on time is field dependent and the switch-off time is device thickness dependent. In contrast, for flexoelectro-optic switching, the response time is controlled by $\gamma_1 p^2/(K_{11} + K_{33})$, where p is the helix pitch and K_{33} is the bend elastic constant, so the switching time is independent of electric field, but strongly dependent on the helical pitch of the material. Nevertheless, in both cases, Equation (4) illustrated that the FoM depends on the ratio of the square of the required retardation to the switching time, and in that sense, comparing the metrics is useful.

There are two key operational bandwidths which can be considered in this experiment. One is the optical spectral

bandwidth over which the device can be operated, the other is the electro-optic switching speed bandwidth. The device is normally designed to operate at a specific wavelength (in our case $\lambda = 633$ nm) where the LC layer with appropriate thickness will work as a half-waveplate and the RM layer in front of the mirror is a quarter-wave thick. Variation in the wavelength (over a spectral bandwidth) will effectively result in errors in the phase modulation and variation in the intensity when switching. The effect of this can be seen in Figure 4. This is shown here as "non ideal" conditions in the layer thicknesses, but is equivalent to changing the wavelength to around 400 nm. As noted, the electro-optic switching speed for the material used in this study was around 500 µs, leading to a 1 kHz bandwidth (assuming an equal duty-cycle switching waveform).

This work has successfully demonstrated an integrated LC optical phase modulator based on the flexoelectro-optic effect of a chiral nematic LC aligned in the ULH mode which exhibits a 2π phase range with a frame rate of 1kHz with the assistance of an additional $\lambda/4$ waveplate placed before the integrated device, which comprises an LC layer consisting of chiral nematic LC and a birefringent polymer film. Although the precise thickness of the whole device was not determined, the approximate thickness of the "working" region can be estimated from the driving voltages. As noted above, a driving voltage of ±34 V is required to achieve ±45° switching across a 5 µm thick layer of material. Therefore, our required driving voltage of ±85 V for the integrated device suggests an overall thickness for the LC layer and waveplate of around 12.5 µm. The operating condition for this device is currently ±85 V at a temperature of 108 °C but could be reduced with further material optimization, such as the mixtures presented in the work of Varanytsia and Chien.[25,26] Additionally, the device we developed shows a response time that is quite fast for analogue phase modulation, with potential operational speeds of more than 1 kHz. This integrated device has substantial potential in spatial light modulator technology, enabling full 2π phase modulation with low-intensity modulation to be achieved. Development into a pixelated spatial light modulator would have a range of applications in optical wave-front engineering and optical light-beam steering in areas such as optical communications.

Experimental Section

Device Fabrication: The procedure employed to fabricate the device is presented schematically in Figure 2. A glass substrate (1 mm-thick) was first cleaned using acetone and a UV Ozone Cleaner (Ossila Corp.) and then coated with a silver film that was approximately 100 nm-thick using thermal evaporation (Syskey Technology Corp.) (1). The thermal evaporator was situated in a glove box (MBraun Labstar) and subjected to a nitrogen atmosphere and an internal pressure of 2×10^{-6} Torr. The deposition was performed at a rate of 0.1 nm s^{-1}, which was monitored using a quartz-oscillation thickness monitor. The silver was deposited through a shadow mask resulting in an active area of approximately 21 mm × 23 mm. After deposition of the silver coating, a thin poly-vinyl alcohol (PVA) layer (PVA was dissolved into water to form a 0.5 wt% PVA solution in water) was deposited on top of the silver film using a spin-coating process at a rate of 1000 rpm for 2 min before being mechanically rubbed with a rubbing machine to form the first of two uniaxial alignment layers for the polymer $\lambda/4$ retarder (2). For the other alignment layer, a second glass substrate was prepared and a thin film of the sulfonic photoalignment material, SD1, was deposited onto the bare glass substrate using spin-coating (2000 rpm, 1 min), which was subsequently aligned through exposure to a polarized UV light source ($\lambda = 365$ nm, power density = 5 mW cm^{-2} and the curing time was 10 mins).[33]

The two substrates were then assembled to form a wedge-cell by using 6 µm spacer beads on one side of the glass substrate and no spacer beads on the other side (the actual wedge spacing was not measured). For the $\lambda/4$ polymer retarder, a reactive mesogen (RM) LC mixture (98 wt% RM257 and 2 wt% IRG819) was opted for, which was capillary filled into the glass cell before being placed on a hot-stage that was set to a temperature of 80 °C. Following this, the sample was exposed to UV light for 40 min at a power density of 100 cm^{-2} to cross-link the RM layer. The device was then soaked in water for one day to dissolve the SD1 layer so that the upper substrate could be removed, leaving a reflective substrate coated with a $\lambda/4$ waveplate (3).

An ITO glass substrate with a photo-aligned SD1 film was prepared while a layer of SD1 was also coated on the top of the polymer film on the mirrored substrate to promote the alignment of the chiral nematic LC. During the process, it was found that the SD1 does not easily spread on top of the polymer film. In order to improve its wettability for SD1, the top surface of the polymer film was treated in a UV Ozone Cleaner (Ossila E511) for 5 min, which ensured that the SD1 could be coated onto it. The two substrates (one was the SD1-coated RM layer substrate and the other was the SD1-coated ITO substrate) were then assembled to form a cell with a wedge geometry in two orthogonal directions: one axis consisted of a wedge in the polymer layer (*y*-axis) whereas the glass substrates were assembled in such a way as to form a wedge along the *x*-axis. Once constructed, the cell was then filled with the chiral nematic mixture, CB7CB + 3 wt% BDH1281 (high twisting power chiral dopant supplied from Merck Ltd.) to form the integrated device (4). The LC mixture was found to exhibit a right-handed chiral nematic phase between 106 and 113 °C (on heating). The pitch (p) of the mixture was found to be approximately $p \approx 210$ nm, which was estimated from the spectral position of the reflection band, measured using a UV–vis spectrometer (Agilent 8454), and the refractive indices quoted in ref. [34] at the measurement temperature. The quality of the ULH texture was investigated using polarizing optical microscopy and was found to be similar to that reported in previously published work.[29] The full device stack showing the orthogonal wedge directions is shown in (5).

Phase Modulation Measurements: The phase modulator device was placed in a Michelson interferometer to measure the optical phase shift as shown in Figure 3. The light source was a continuous wave Helium–Neon (He–Ne) laser (Uniphase 1125P) that generated light at a wavelength of 632.8 nm. The input light first passed through a non-polarizing beam-splitter (Newport 05BC16NP) via the aid of mirrors before being split into two components. One of the output beams from the beam-splitter (the signal beam) passed through the integrated device and is reflected back toward the beam-splitter. As the chiral nematic phase of the device was at elevated temperatures (between $T = 106$ and 113 °C), a temperature-controlled hot-stage was required to allow it to be operated in the chiral nematic phase. The LC layer was aligned in the ULH geometry (with SD1 working as the alignment layer) by cooling from the isotropic phase in the presence of an electric field (≈2 V μm^{-1}) and mechanically rubbing the device with a blunt instrument to promote the lying helix alignment. Monodomains of ULH alignment were found to be 150×150 μm^2 in size, in accordance with the results presented in a previous study for a comparable LC layer (in this experimental device the ULH alignment was not stabilized by a polymer network).[29] Before the integrated LC device, a linear polarizer and $\lambda/4$ waveplate were included to generate circularly polarized light before a lens L1 focused the incoming light into a monodomain region of the device. The other output beam (the reference beam) was directed toward two mirrors to reflect the light back with a small angle offset so as to generate clear interference fringes at the CCD camera. The fringes were captured by using a collection lens to image directly onto a CCD camera (Thorlabs DCU224C, 1280 × 1024, 8-bit color). The fringe period was estimated from the small angle introduced between the signal and reference beams of the Michelson interferometer to be approximately 30 µm, resulting in a number of fringes across any individual ULH domain.

An arbitrary function generator (Wavetek 395) was used to drive the flexoelectro-optic switching through an additional voltage amplifier (FLC Electronics F10AD). For this study, the voltage signal applied to the integrated device was a 1 kHz square-wave with a controllable amplitude level. The CCD camera was set to have a shutter time that was substantially less than one-half of the square wave period (i.e., less than 500 µs) and the frame rate was adjusted to be close to (but not identical to) a subharmonic of the 1 kHz device driving frequency. This then enabled the interference fringes to be observed through a sub-sampling (aliasing) effect. Taking line samples from the images and fitting to these allowed the phase modulation to be determined. All subsequent measurements were conducted at a temperature of $T = 108$ °C for which the sample was in the chiral nematic phase and a switching angle of ±45° was observed for an applied voltage of ±85 V.

Acknowledgements

The authors gratefully acknowledge the Engineering and Physical Sciences Research Council (UK) for financial support through grant numbers EP/M017923/1, EP/M015726/1, and EP/M016218/1, as well as the European Space Agency (ESA) through contract 4000125232/18/NL/AR/zk. T.A. would like to thank the Punjab Educational Endowment Fund (Pakistan) for financial support during his graduate studies.

Conflict of Interest

The authors declare no conflict of interest.

Keywords

chiral nematic liquid crystal, flexoelectricity, phase modulator, spatial light modulator

Received: June 17, 2020
Revised: September 22, 2020
Published online:

[1] A. Jesacher, C. Maurer, A. Schwaighofer, S. Bernet, M. Ritsch-Marte, *Opt. Express* **2008**, *16*, 2597.
[2] A. Jesacher, M. Booth, *Opt. Express* **2010**, *18*, 21090.
[3] Y. Xie, W. Wang, H. Chen, A. Konneker, B.-I. Popa, S. A. Cummer, *Nat. Commun.* **2014**, *5*, 5553.
[4] A. M. Weiner, *Rev. Sci. Instrum.* **2000**, *71*, 1929.
[5] T. Gould, D. Burke, J. Bewersdorf, M. Booth, *Opt. Express* **2012**, *20*, 20998.
[6] M. Wu, O. Solgaard, J. Ford, *J. Lightwave Technol.* **2006**, *24*, 4433.
[7] Z. Zhang, Z. You, D. Chu, *Light: Sci. Appl.* **2014**, *3*, e213.
[8] G. Lazarev, S. Bonifer, P. Engel, D. Höhne, G. Notni, *Proc. SPIE* **2017**, *2017*, 103351B.
[9] N. Collings, J. Gourlay, D. G. Vass, H. J. White, C. Stace, G. M. Proudley, *Appl. Opt.* **1995**, *34*, 5928.
[10] S. Broomfield, M. Neil, E. Paige, *Appl. Opt.* **1995**, *34*, 6652.
[11] Y. Wang, F. Zhang, X. Tang, X. Chen, Y. Chen, W. Huang, Z. Liang, L. Wu, Y. Ge, Y. Song, J. Liu, D. Zhang, J. Li, H. Zhang, *Laser Photonics Rev.* **2018**, *12*, 1800016.
[12] L. Lu, W. Wang, L. Wu, X. Jiang, Y. Xiang, J. Li, D. Fan, H. Zhang, *ACS Photonics* **2017**, *4*, 2852.
[13] M. Zhang, Q. Wu, F. Zhang, L. Chen, X. Jin, Y. Hu, Z. Zheng, H. Zhang, *Adv. Opt. Mater.* **2019**, *7*, 1800224.
[14] Y. Wang, W. Huang, C. Wang, J. Guo, F. Zhang, Y. Song, Y. Ge, L. Wu, J. Liu, J. Li, H. Zhang, *Laser Photonics Rev.* **2019**, *13*, 1800313.
[15] S. Reichelt, R. Häussler, G. Fütterer, N. Leister, H. Kato, N. Usukura, Y. Kanbayashi, *Opt. Lett.* **2012**, *37*, 1955.
[16] J. Chen, S. M. Morris, T. D. Wilkinson, J. P. Freeman, H. J. Coles, *Opt. Express* **2009**, *17*, 7130.
[17] J. S. Patel, R. B. Meyer, *Phys. Rev. Lett.* **1987**, *58*, 1538.
[18] P. Rudquist, L. Komitov, S. T. Lagerwall, *Phys. Rev. E* **1994**, *50*, 4735.
[19] P. Rudquist, L. Komitov, S. T. Lagerwall, *Liq. Cryst.* **1998**, *24*, 329.
[20] P. Rudquist, T. Carlsson, L. Komitov, S. T. Lagerwall, *Liq. Cryst.* **1997**, *22*, 445.
[21] J. Harden, B. Mbanga, N. Éber, K. Fodor-Csorba, S. Sprunt, J. T. Gleeson, A. Jákli, *Phys. Rev. Lett.* **2006**, *97*, 157802.
[22] R. Meyer, *Phys. Rev. Lett.* **1969**, *22*, 918.
[23] J. A. J. Fells, X. Wang, S. J. Elston, C. Welch, G. H. Mehl, M. J. Booth, S. M. Morris, *Opt. Lett.* **2018**, *43*, 4362.
[24] X. Wang, J. A. J. Fells, W. C. Yip, T. Ali, J.-D. Lin, C. Welch, G. H. Mehl, M. Booth, T. D. Wilkinson, S. M. Morris, S. J. Elston, *Sci. Rep.* **2019**, *9*, 7016.
[25] A. Varanytsia, L.-C. Chien, *Sci. Rep.* **2017**, *7*, 41333.
[26] A. Varanytsia, L.-C. Chien, *J. Appl. Phys.* **2016**, *119*, 014502.
[27] V. Joshi, K.-H. Chang, A. Varanytsia, D. A. Paterson, J. M. D. Storey, C. T. Imrie, L. C. Chien, *Adv. Opt. Mater.* **2018**, *6*, 1800013.
[28] X. Wang, J. A. J. Fells, C. Welch, M.-G. Tamba, G. H. Mehl, S. M. Morris, S. J. Elston, *Liq. Cryst.* **2019**, *46*, 408.
[29] J. A. J. Fells, C. Welch, W. C. Yip, S. J. Elston, M. J. Booth, G. H. Mehl, T. D. Wilkinson, S. M. Morris, *Opt. Express* **2019**, *27*, 15184.
[30] S. Bolis, C. Tartan, J. Beeckman, P. Kockaert, S. Elston, S. Morris, *Liq. Cryst.* **2018**, *45*, 774.
[31] I. C. Khoo, S. T. Wu, *Optics and Nonlinear Optics of Liquid Crystals*, World Scientific, Singapore **1993**.
[32] E. Jakeman, E. P. Raynes, *Phys. Lett. A* **1972**, *39*, 69.
[33] O. Yaroshchuk, Y. Reznikov, *J. Mater. Chem.* **2012**, *22*, 286.
[34] G. Babakhanova, Z. Parsouzi, S. Paladugu, H. Wang, Y. Nastishin, S. Shiyanovskii, S. Sprunt, O. Lavrentovich, *Phys. Rev. E* **2017**, *96*, 062704.